INTERNATIONAL JOURNAL OF HYDROGEN ENERGY 40 (2015) 4558–4566

Available online at www.sciencedirect.com

ScienceDirect

journal homepage: www.elsevier.com/locate/he

Enhanced photocatalytic activity of palladium decorated TiO_2 nanofibers containing anatase-rutile mixed phase

Ming-Chung Wu[*], *Pei-Huan Lee*, *Dai-Lung Lee*

Department of Chemical and Materials Engineering, College of Engineering, Chang Gung University, Taoyuan 33302, Taiwan

ARTICLE INFO

Article history:
Received 24 October 2014
Received in revised form
29 December 2014
Accepted 2 January 2015
Available online 4 March 2015

Keywords:
TiO_2
Nanostructures
Photocatalyst
Photodegradation
Photocatalytic hydrogen generation

ABSTRACT

Titanium dioxide (TiO_2) based material is probably the most promising environmentally friendly photocatalyst, with low cost, high photocatalytic activity, and excellent photostability as demonstrated in photocatalytic hydrogen generation and in abatement of organic pollutant. In this study, sodium hydrogen titanate nanofibers were prepared by alkaline hydrothermal synthesis at first. Then, a quick screening was carried out to find the appropriate calcination condition for preparing the high catalytically active titanium dioxide nanofibers (TiO_2 NFs) with anatase-rutile mixed phase (anatase-rutile TiO_2 NFs). The crystalline structure of anatase-rutile TiO_2 NFs was analyzed by Raman spectrometer and X-ray diffraction meter. The anatase-rutile TiO_2 NFs calcined at 800 °C for 4 h shows the highest decomposition rate of the brilliant green, higher than that of the commercial photocatalyst – Degussa P25. Furthermore, palladium based nanoparticles was decorated on the surface of anatase-rutile TiO_2 NFs to enhance the photocatalytic hydrogen performance. We also developed a method to make use of catalyst materials for large-area coatings and freestanding films by preparing the cellulose/catalyst composite films. The obtained catalysts in this study might be a reasonable alternative for the commercial TiO_2, Degussa P25, for photocatalytic applications in the decomposition of organic dyes and photocatalytic hydrogen generation.

Introduction

In recent years, energy and environmental issues are significant topics around the world. The discovery of photoelectrochemical splitting of water on titanium dioxide (TiO_2) by Fujishima and Honda in 1972 has initiated a considerable boom of semiconductor-based photocatalyst research [1]. TiO_2 is the subject of intensive research as the most promising photocatalyst because of its good photocatalytic activity and excellent photostability, at the same time being environmentally friendly and low cost [2,3]. In addition. TiO_2 can also be used to address several aspects of modern renewable energy production, such as efficient solar cell electrode [4,5], photocatalytic hydrogen production [6–8], and management of environmental pollution [9,10]. TiO_2 is a wide-band-gap

* *Corresponding author*. Tel.: +886 3 2118800x3545; fax: +886 3 2118800x5324.
E-mail address: mingchungwu@mail.cgu.edu.tw (M.-C. Wu).
http://dx.doi.org/10.1016/j.ijhydene.2015.01.012

semiconducting material with several natural crystalline phases, such as anatase, rutile, brookite, and etc. [11,12] Actually, some literatures demonstrated that the photocatalytic activity of anatase/rutile mixed phase is higher than single phase (anatase or rutile) due to the formation of barrier between the anatase and rutile surface to enhance the electron–hole separation rate [13–16]. The alkaline hydrothermal synthesis has opened new possibilities for large scale and simple production of various types of titanate nanostructures such as nanoparticle, nanofiber, and nanotube [17,18]. The titanates can be used as the starting materials for the synthesis of nanostructured highly photoactive TiO_2-based materials by a simple thermal annealing process [19–21]. TiO_2 Degussa P25 with an anatase/rutile ratio of 80/20 is a widely used commercial photocatalyst because of its relatively high level of activity in many photocatalytic reaction systems [22]. Actually, it is not easy to find a photocatalyst showing activity higher than that of TiO_2 P25, so it has been used as a standard TiO_2 photocatalyst [23–25]. Developing a material as a reasonable alternative for TiO_2 P25 is the basic goal for the development of novel photocatalyst.

TiO_2 contacted with large work function metal nanoparticles results in Schottky barrier at the interface. At first, a consequence of photopromoted electrons preferentially migrates from the conduction band of TiO_2 to the metal nanoparticles, thus decreasing electron–hole recombination. Then, the efficient charge separation was induced by the Schottky interface between metal nanoparticles and n-type semiconducting TiO_2. Finally, protons formed by the reaction between holes and water are reduced by electrons injected previously into the metal nanoparticles. This is due to electrons being restricted in the metal nanoparticle by the Schottky barrier, preventing the undesired electron–hole recombination [26–29]. It has been found to enhance the photocatalytic performance by decorations of TiO_2 with carbon nanotubes [30], graphene [31], metals, and metal oxides such as Pt [27,32,33], Au [34], Pd [27,32,34], PdO [35], Ni [36], and Ag [37,38]. However, using noble metal to decorate TiO_2 catalysts is still an effective method to obtain the high activity photocatalysts. Ismail et al. reported the synthesis of a highly active photocatalyst of mesoporous PdO–TiO_2 material using different PdO concentration through simple one-step sol–gel reactions. Pd^{2+}-ions have been immobilized into TiO_2 networks by cross linking triblock copolymer as the structure-directing agents to develop highly efficient PdO–TiO_2 photocatalysts. The measured photonic efficiency is as high as 19.5% [35]. Besides, Roy et al. reported a synthesis of $Ti_{1-x}Pd_xO_{2-\delta}$ crystallizing in anatase phase with Pd^{2+}-ion, showing that enhanced CO oxidation at Pd^{2+} ion site and O_2 or NO photo dissociation at oxide ion vacancy is responsible for the enhanced catalytic activity [39]. Palladium (Pd) is the cheapest and most commonly used metal among the noble metals for co-catalyst with the TiO_2 photocatalyst, and the cost of Pd metal is approximately 20–25% of that of platinum (Pt) metal.

Thermal treatments carried out in hydrogen for co-catalyst could be an useful method for enhancing the photocatalytic activity, but it also could influence the crystalline and electronic structure of TiO_2 thus inducing a bandgap narrowing [40,41]. Hence, the reduce process could cause the change between TiO_2 and metal nanoparticles at the same time. However, highly-crystalline TiO_2 usually could not be reduced by hydrogen in normal pressure [42].

Herein, in order to prepare the catalytically active TiO_2 NFs from SHT NFs, a quick screening was carried out to find the appropriate calcination temperature. The obtained anatase-rutile TiO_2 NFs calcined at 800 °C shows the highest photocatalytic activity among the thermally treated TiO_2 NFs. Then, we prepared palladium decorated TiO_2 NFs (TiO_2–Pd NFs) by wet impregnation method followed by hydrogen-thermal reduction process in order to enhance the photocatalytic activity. The obtained TiO_2–Pd NFs reduced at 300 °C might be a reasonable alternative for the traditional TiO_2 P25 for photocatalytic applications in the decomposition of organic dyes and photocatalytic hydrogen generation.

Experimental details

Preparation of palladium decorated TiO_2 nanofibers

For the preparation of sodium hydrogen titanate nanofibers (SHT NFs), we suspend 2.50 g TiO_2 anatase powder (Aldirch, 98%) in 62.5 mL of 10.0 M NaOH aqueous solution, followed by a treatment in a Teflon-lined autoclave at 150 °C for 24 h, applying revolving around its short axis. Then, the product, sodium titanate nanofibers, was then washed in 0.10 M HCl to exchange sodium ions for protons. The neutralized product was washed with deionized water and finally filtered and dried in the air at 70 °C. In order to prepare the TiO_2 NFs, the SHT NFs were calcined in the air at various temperatures, 400, 550, 600, 700, 800 and 950 °C, respectively, with heating rate of 5 °C/min for 4 h to find the optimal calcination temperature. For TiO_2–Pd NFs, 29.2 mg of palladium(II) acetylacetonate (Aldrich, 99%) was dissolved in 200 mL of acetone and mixed with 1.0 g of TiO_2 NFs by ultrasonic agitation for 3 h. Then, the mixture was stirred for 6 h. After evaporating the solvent at ~80 °C under N_2 atmosphere, the samples were calcined in the air at 300 °C for 2 h, and then reduced at various temperature, such as 300, 400 and 500 °C, in 15% H_2 (in N_2 buffer) flow for 4 h to obtain TiO_2–Pd NFs with ~1.0 wt% metal loading.

Characterization

In order to obtain the Raman scattering spectra, anatase TiO_2 (Acros, TiO_2, anatase powder, 98+%), rutile TiO_2 (Alfa Aesar, TiO_2, rutile powder, 99.5%) and various thermally treated TiO_2 NFs were positioned on a high-resolution piezoelectric stage of the scanning microscopy (WITec, Alpha300S, Germany) and excited by a 632.8 nm He–Ne laser. The laser beam was focused with a 10X objective lens (Nikon plane objective, NA ~ 0.9), and the diameter of the laser beam focus was about 10 μm. The crystal structures of various thermally treated TiO_2 NFs were determined by X-ray diffraction spectrometry (XRD) (Rigaku, TTRAXIII, Japan) using Cu K_α radiation at 50 kV and 300 mA. XRD patterns were collected from 2θ between 10 and 80 with a 0.005° step at 5 min^{-1}. The microstructure and morphology of various thermally treated TiO_2 NFs were studied by scanning electron microscopy (SEC, SNE-4500M MiniSEM, Korea).

Photocatalytic activity testing

The photodegradation of organic dye behaviors of TiO_2 P25 (Degussa) and TiO_2-based materials were performed by monitoring the decoloration of brilliant green. In a typical experiment, 20.0 mg of catalyst was sonicated for 5 min in 150 mL brilliant green aqueous solution (20 mg/L). The suspension was irradiated with UV-B light (Sankyo Denki, G8T5E, 8 W × 6 sets) under vigorous stirring at ambient conditions. After a centrifuging process (15 min at 3500 rpm), the UV–Vis spectrum of the remained brilliant green and its derivatives in the supernatant was recorded in the spectral range from 400 nm to 900 nm (Jasco Analytical Instruments, V-650 UV–Vis Spectrophotometer). The brilliant green concentration was calculated from the absorbance at $\lambda = 624$ nm, extrapolated to a previously plotted calibration curve.

Hydrogen generation from ethanol–water mixtures

Photocatalytic water splitting hydrogen generation tests were carried out by using 1:1 volume ratio mixture of ethanol and water (total 2.0 L), in which 10.0 mg of TiO_2-based catalyst was suspended before each experiment. The temperature of the mixture was kept near the room temperature. For light source, six pieces of UV-B lamps (Sankyo Denki G15T8E UV-B lamp, the wavelength of maximum emission of UV-B lamp was ~312 nm, and the power was 8.0 W) were placed in a hexagonal arrangement around the reactor. To avoid sedimentation of the catalyst powders, nitrogen (99.995%) was bubbled through the reactor with a flow rate of 400 mL/min, serving also as a purging gas for the evolving gaseous products. The outlet of the reactor was connected a cold trap, a molecular sieve, and a hydrogen analyzer (Status Scientific Controls Ltd, FGD3).

Results and discussion

In order to prepare the high catalytically TiO_2 NFs from SHT NFs, a quick screening was carried out to find the suitable calcination temperature. Anatase TiO_2, rutile TiO_2 and SHT NFs calcined at various temperatures were identified by Raman spectrometer. The Raman spectra of anatase TiO_2 and rutile TiO_2 are as standard. The spectra presented several TiO_2 phases, such as anatase, rutile, and mixed phase, as shown in Fig. 1. The TiO_2 NFs samples prepared from SHT NFs calcined at various temperatures for 4 h were denoted as TiO_2-xxx NFs, for which "xxx" indicating various clacination temperatures. Raman spectra showed that samples calcined below 400 °C presented a mixed phase of amorphous phase and anatase. When the calcination temperature went above 550 °C, the crystal phase transformed to anatase. The anatase TiO_2 showed major Raman bands at 144, 200, 398, 515,517 and 640 cm^{-1}, but the Raman band at 515 cm^{-1} was superimposed with the 517 cm^{-1} band. These bands can be attributed to the six Raman-active modes of anatase phase with the symmetries of E_g, E_g, B_{1g}, A_{1g}, B_{1g}, and E_g, respectively [43]. When calcination temperature went above 800 °C, TiO_2 NFs sample presented rutile phase with their major Raman bands at 448 and 617 cm^{-1}. For rutile TiO_2, the typical Raman bands appear

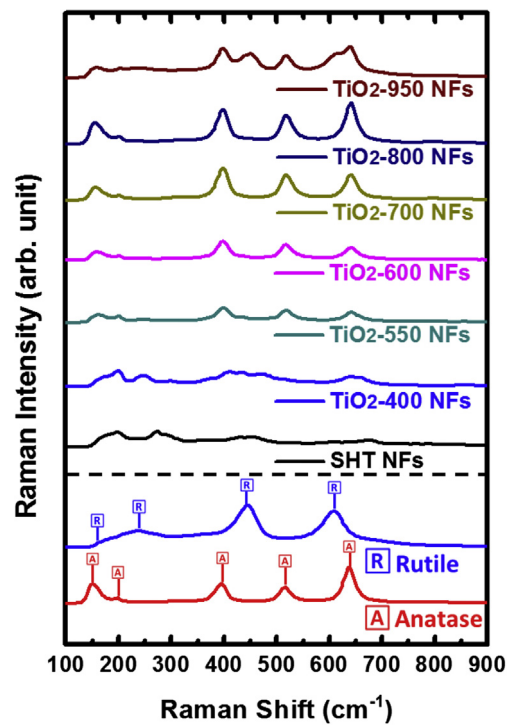

Fig. 1 – Raman spectra of anatase TiO_2, rutile TiO_2, SHT NFs and SHT NFs calcined at various temperatures, 400, 550, 600, 700, 800 and 950 °C, for 4 h.

at 143, 243, 448 and 617 cm^{-1}, which can be ascribed to the B_{1g}, two-phonon scattering, E_g, and A_{1g} modes of rutile phase, respectively [43].

The XRD pattern of the synthesized SHT NFs is similar to our previous work [27,32]. SHT NFs treated with 4 h of various calcination temperatures in the air were measured by XRD as shown in Fig. 2(a). The X-ray diffraction patterns of the thermally treated SHT NFs showed an obvious phase transformation. With calcination temperatures of up to 550 °C, there was only formation of anatase phase. The intensity of reflections increased as the calcination temperature increased, indicating better ordering of the lattice. However, at calcination temperatures of above 800 °C, the formation of TiO_2 rutile phase started, as shown by the appearance of its (110) reflection at ~27.4° of 2θ (Fig. 2(b)). The crystalline structure of TiO_2-800 NFs and TiO_2-950 NFs are the mixture of anatase and rutile phase. The XRD result was consistent with the results of Raman measurement.

The photocatalytic activities of the synthesized TiO_2 NFs were tested with UV-B light-induced photodegradation of brilliant green in aqueous solution. UV–vis spectra of brilliant green as a function of UV light irradiation time were recorded. From the absorbance measured at $\lambda = 624$ nm, the corresponding dye concentrations were calculated using a calibration curve measured previously. The overall order of photodegradation activity was TiO_2-800 NFs > Degussa P25 > TiO_2-700 NFs > TiO_2-600 NFs > TiO_2-950 NFs > TiO_2-400 NFs as shown in Fig. 3(a), indicating that TiO_2-800 NFs had the highest photodegradation activity. TiO_2-800 NFs containing

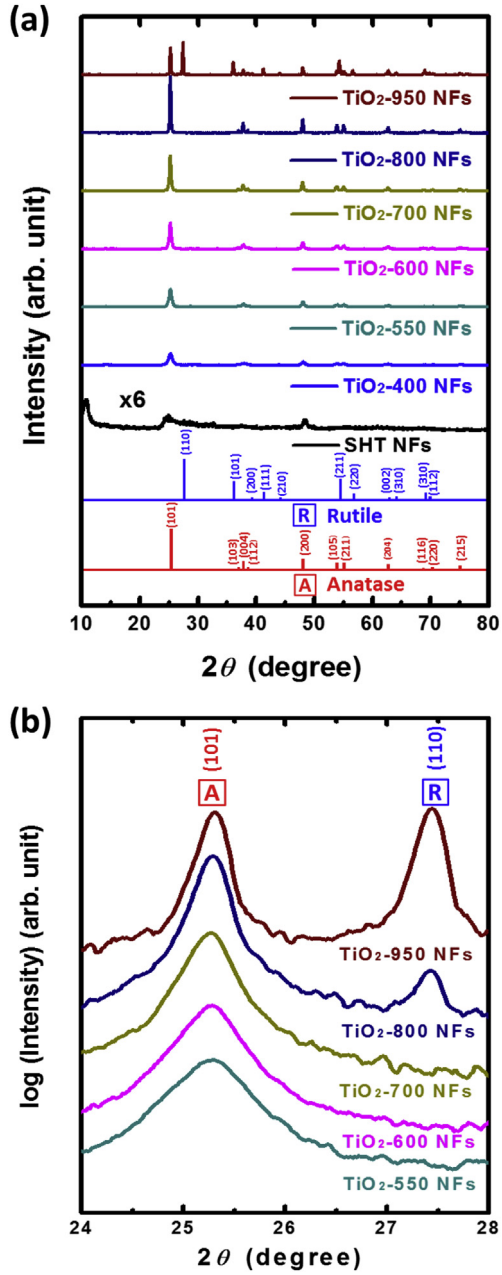

Fig. 2 – X-ray diffraction patterns of SHT NFs and SHT NFs calcined in the air at 400, 550, 600, 700, 800 and 950 °C for 4 h (A = Anatase; R = Rutile).

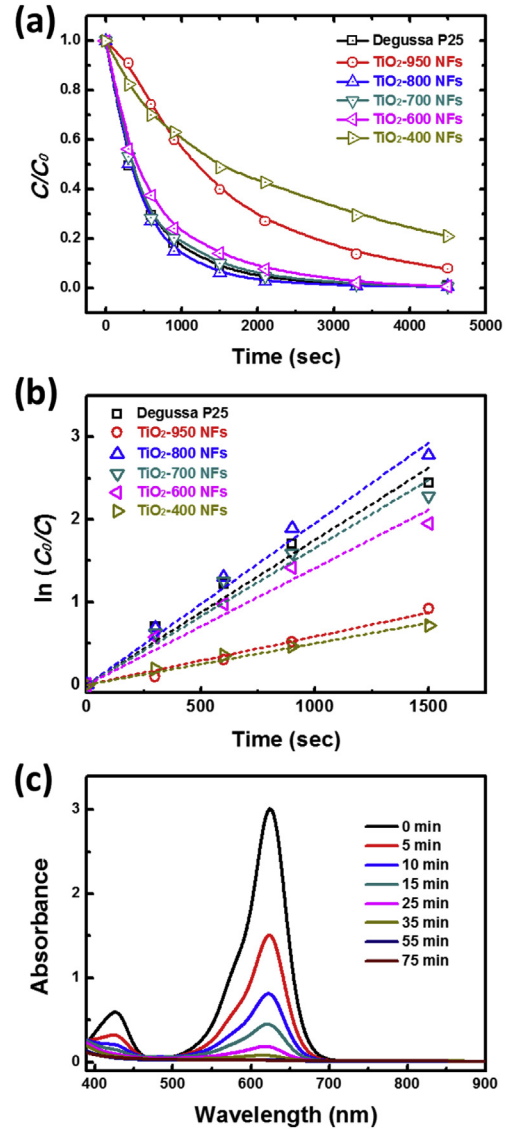

Fig. 3 – (a) Photocatalytic activities of TiO_2 NFs calcined at various temperatures over the photodegradation of brilliant green under UV-B irradiation. (b) Linearized kinetic plots for the degradation of brilliant green using various types of TiO_2 NFs based catalysts. (c) Absorbance spectra of brilliant green (initial concentration of 20.0 mg/L) as a function of illumination time with TiO_2-800 NFs (20.0 mg dispersed in 150 mL of solution). (For interpretation of the references to color in this figure legend, the reader is referred to the web version of this article.)

anatase-rutile mixed phase exhibited the highest photodegradation activity due to the efficient charge separation at the interface between anatase TiO_2 and rutile TiO_2. Because the energy levels of both conduction band and valence band on rutile TiO_2 are higher than those on anatase TiO_2, it generated a barrier between anatase TiO_2 and rutile TiO_2, which can separate photogenerated electrons and holes easily. On the other hand, the electron–hole recombination rates of single phase TiO_2 are larger than TiO_2 with anatase-rutile mixed phase. TiO_2-catalyzed photodegradation of different dyes essentially follow Langmuir–Hinshelwood kinetics, which can be simplified to an apparent first-order kinetics at lower initial brilliant green concentrations, mathematically described as $ln(C_0/C) = kt$; where C is the concentration of the dye at time t, C_0 is the initial concentration, and k is the apparent reaction rate constant [27,44]. Plotting the logarithm of the reciprocal of brilliant green concentrations as a function of time, we obtained linear slopes for each catalyst studied and they were in good agreement with the

Langmuir–Hinshelwood model. TiO_2-800 NFs and Degussa P25 gave the fast decoloration phenomenon for photodegradation of brilliant green, and their calculated rate constants were ~1.96×10^{-3} s^{-1} and ~1.75×10^{-3} s^{-1}, respectively. In Fig. 3(b), TiO_2-800 NFs showed higher photocatalytic activity than Degussa P25. TiO_2-800 NFs consisting a mixed phase of anatase and rutile may be a reasonable alternative of the traditional Degussa P25 for photocatalytic applications. The UV–vis absorbance spectra for UV-B light-induced photodegradation of brilliant green in aqueous solution as a function of illumination time with TiO_2-800 NFs were shown in Fig. 3(c).

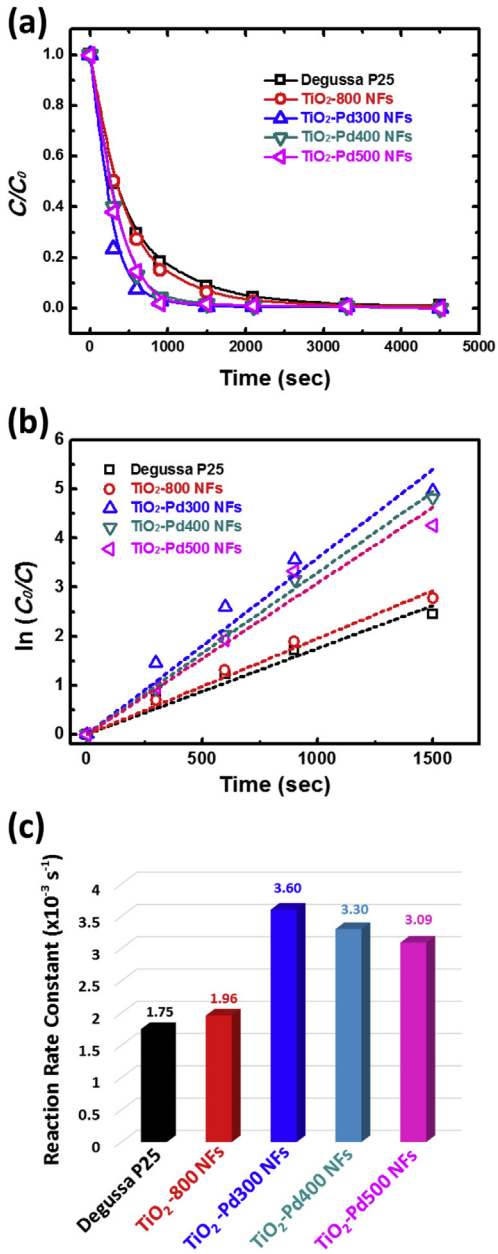

Fig. 4 – (a) Photocatalytic activities of TiO_2–Pd NFs reduced at various temperatures over the photodegradation of brilliant green under UV-B irradiation. (b) Linearized kinetic plots for the degradation of brilliant green using various types of TiO_2–Pd NFs based catalyst. (c) The bar charts of photodegradation reaction rate constants of P25, TiO_2 NFs and various TiO_2–Pd NFs based catalysts. (For interpretation of the references to color in this figure legend, the reader is referred to the web version of this article.)

In order to enhance the performance of photodegradation toward organic dye and photocatalytic hydrogen generation, TiO_2-800 NFs decorated with Pd-based nanoparticles was prepared because of palladium is the cheap and most commonly used metal among the noble metals for co-catalyst with TiO_2 photocatalyst. The mechanism of photodegradation of brilliant green in aqueous solution is shown in Eqns. (1)–(7) [2,45].

$$TiO_2 + h\nu \rightarrow h^+ (TiO_2) + e^-(\text{metal}) \quad (1)$$

$$O_2 + e^- (\text{metal}) \rightarrow O^{2-} \quad (2)$$

$$O^{2-}\ O^{2-} + H^+ \rightarrow HO_2 \quad (3)$$

$$H_2O + h^+ (TiO_2) \leftrightarrow OH \quad (4)$$

$$OH^- + h^+ (TiO_2) \leftrightarrow OH \quad (5)$$

$$OH + \text{organic dye} \rightarrow CO_2 + H_2O \quad (6)$$

$$HO_2 + \text{organic dye} \rightarrow CO_2 + H_2O \quad (7)$$

Samples prepared from Pd-based nanoparticles decorated TiO_2-800 NFs were reduced at various temperatures for 4 h. These samples were denoted as TiO_2-Pdyyy NFs, for which "yyy" indicating various reduction temperatures of 300, 400, and 500 °C, respectively. Photocatalytic activities of TiO_2–Pd NFs reduced in N_2/H_2 atmosphere at various temperatures were measured. The results were shown in Fig. 4(a). Among Pd

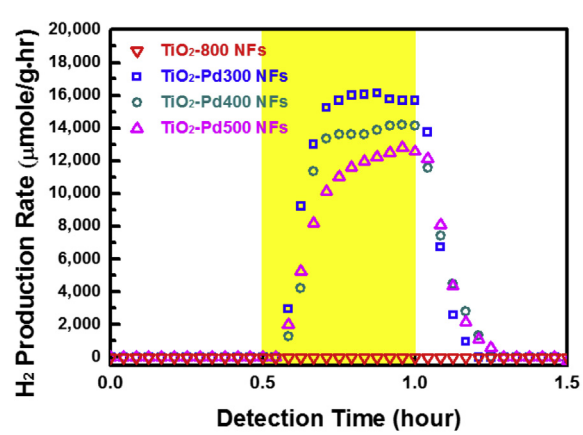

Fig. 5 – Photocatalytic hydrogen production rates of TiO_2-800 NFs and TiO_2–Pd NFs with various reduction temperatures under the irradiation of UV-B lamp.

decorated TiO_2 NFs based catalysts, TiO_2–Pd300 NFs exhibited the highest photodegradation activity of brilliant green with a calculated rate constant of ~3.60 × 10^{-3} s^{-1} as shown in Fig. 4(b). The photocatalytic activity decreased as the reduction temperature increased for the TiO_2–Pd NFs based catalysts. Hence, the reduction temperature of 300 °C is enough for preparing the TiO_2–Pd NFs based catalyst with high photocatalytic performance, because of the chemical state of palladium plays an important role for the preparation of high performance catalysts. TiO_2–Pd300 NFs is suitable for the applications of photodegradation of brilliant green, and its UV–vis absorbance spectra of brilliant green in aqueous solution for UV-B light-induced photodegradation as a function of illumination time were shown in Fig. 4(c).

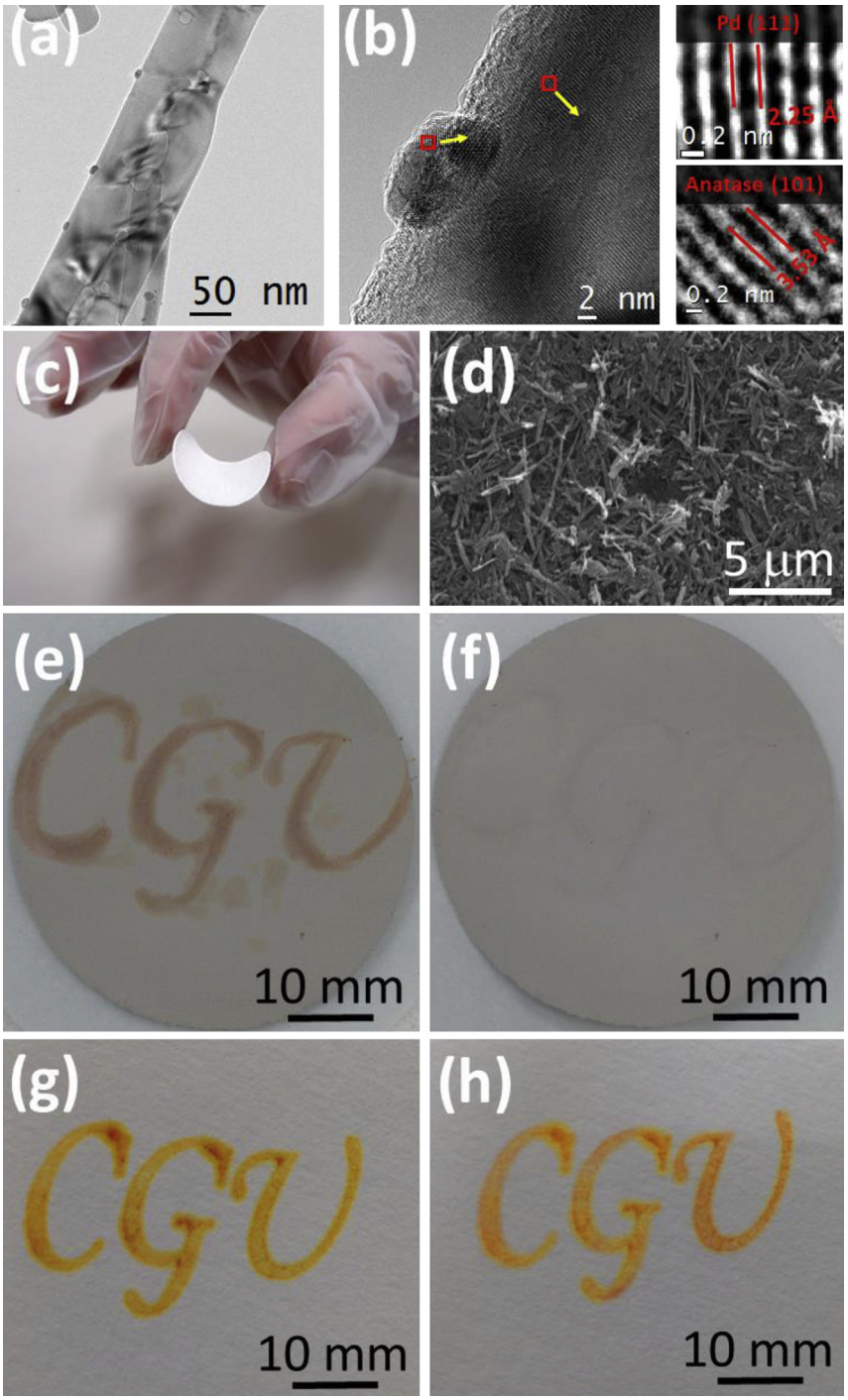

Fig. 6 – (a) TEM images of TiO_2–Pd300 NFs. (b) The high-resolution TEM image of TiO_2–Pd300 NFs, and the high-magnification lattice images of Pd-based nanoparticles (top) and TiO_2 NFs (bottom). (c) Photograph of a bent TiO_2-800 NFs composite membrane, and (d) SEM image of cellulose/TiO_2–Pd300 NFs surface. The photographs of three letters "CGU" affixed on (e) the composite membrane, (f) the composite membrane after 1.0 h of UV-B exposure, (g) a piece of paper, and (h) a piece of paper after 1.0 h of UV-B exposure.

Photocatalytic hydrogen production rates of TiO_2-800 NFs and TiO_2–Pd NFs with various reduction temperatures, such as 300, 400 and 500 °C, under the irradiation of UV-B lamp are shown in Fig. 5. For pure TiO_2 materials without metal decoration, it is not active in the photocatalytic hydrogen generation, and must be combined with a precious transition metal to yield an active photocatalyst. The purpose of metal nanoparticle decorated on TiO_2 surface is to generate a Schottky barrier at the interface between TiO_2 and metal nanoparticles. The highest hydrogen production rate was found with TiO_2–Pd300 NFs under UV-B irradiation with a rate of as high as 16,200 μmol/g·hr. Moreover, the photocatalytic hydrogen production rate was found to be around 14,300 μmol/g·hr for TiO_2–Pd400 NFs, and 12,900 μmol/g·hr for TiO_2–Pd500 NFs. The photocatalytic hydrogen production rate decreased as the reduction temperature increased for TiO_2–Pd NFs based catalysts. In our previous study [46], the chemical state of Pd (Pd, PdO, and Pd^{2+}-ion) plays an important role for photocatalytic hydrogen production, because of its ability to capture the photogenerated electrons effectively and to reduce the rate of electron–hole recombination. The hydrogen reduction time increase, the amount of Pd and PdO increase, but the amount of Pd^{2+}-ion decrease. Pd-based nanoparticle decorations with the appropriate chemical states on TiO_2–Pd300 NFs surface could capture the photogenerated electrons effectively and could reduce the rate of electron–hole recombination to enhance the photocatalytic hydrogen production rate. This is due to electrons being restricted in the metal nanoparticle by the Schottky barrier, preventing the undesired electron–hole recombination.

TEM images of TiO_2–Pd300 NFs were shown in Fig. 6(a). The length of TiO_2 NFs was up to a few micrometers and its diameter was ranged from 80 to 150 nm. Pd-based nanoparticles distributed on the surface of TiO_2 NFs presented uniform size distribution with average particle diameters of 7.3 ± 1.3 nm, and (111) crystal plane is 2.25 Å as shown in Fig. 6(b). The (101) crystal plane of TiO_2 was observed for TiO_2–Pd300 NFs, and the (101) spacing is 3.53 Å. Next, we used cellulose and the TiO_2-800 NFs to prepare composite films that enabled handling for easy-recycling applications as shown in Fig. 6(c). The presence of TiO_2 with different shapes in the different types of catalyst materials can influence mechanical friction and sticking of adjacent cellulose fibers coated with the nanoparticles, thus, affecting flexibility. Fig. 6(d) showed the cellulose microfibers were uniformly coated with the TiO_2 NFs. Using photocatalysts to degrade organic compounds on surfaces has attracted considerable attention in recently years, due to the possible applications in self-cleaning coatings and antimicrobial surfaces. Here, we also used cellulose and TiO_2–Pd300 NFs to prepare freestanding composite membranes that enabled easy handling. Using the photocatalyst composite films we demonstrated degradation of organic dyes deposited on the surface of thin catalyst membranes as shown in Fig. 6(e–h). Three letters "*CGU*" were affixed on a TiO_2–Pd300 NFs composite film (Fig. 6(e)) and a piece of paper (Double A, 80 gsm) (Fig. 6(g)) by a stamp with a highlight pen ink (Simbalion, FM-35), respectively. Then, these two samples were exposed to UV-B light for 1.0 h. The composite membranes consisting of cellulose and TiO_2–Pd300 NFs showed obvious changes in the intensity of the color pattern as shown in Fig. 6(f). The original stain could hardly be seen, indicating that the fading of the dye was practically complete. However, it just exhibits minor changes for the "*CGU*" on the paper for the stain on the paper, as shown in Fig. 6(h), because no catalyst to improve the photocatalytic degradation of organic dye.

Conclusion

In summary, this study included: (i) photodegradation of brilliant green with TiO_2 NFs and TiO_2–Pd NFs, (ii) photocatalytic hydrogenation of TiO_2 NFs and TiO_2–Pd NFs, and (iii) degradation of organic dyes with freestanding membranes containing cellulose and TiO_2 NFs. At first, SHT NFs calcined at 800 °C for 4 h leads to the formation of anatase-rutile TiO_2 NFs. Compared with other TiO_2 based catalysts, the brilliant green decoloration using TiO_2–Pd300 NFs shows the highest photocatalytic activity. In addition, TiO_2–Pd300 NFs also exhibits the highest H_2 production rate at 16,200 μmol/g·hr. In both cases, TiO_2–Pd300 NFs has proven to be more efficient. This can be explained by the formation of nano-sized Schottky interfaces at the contacts between TiO_2 and metal nanoparticles. Furthermore, the ability to fabricate cellulose/TiO_2–Pd300 NFs composite membrane was developed for utilizing photocatalyst materials in freestanding films. The obtained TiO_2–Pd300 NFs may be a reasonable alternative of the commercial Degussa P25 for photocatalytic applications in the decomposition of organic dyes and photocatalytic hydrogen generation.

Acknowledgments

Financial support obtained from Ministry of Science and Technology of Taiwan (MOST 102-2633-E-182-001, MOST 103-2221-E-182-008-MY2 and MOST 104-3113-E-002-010) and Chang Gung University Research Project is highly appreciated. We appreciate Prof. Wei-Fang Su at National Taiwan University and Dr. Ming-Tao Lee group (BL-13A1) at National Synchrotron Radiation Research Center for useful discussion and suggestions.

REFERENCES

[1] Fujishima A, Honda K. Electrochemical photolysis of water at a semiconductor electrode. Nature 1972;238:37–8.
[2] Rawal SB, Bera S, Lee D, Jang D, Lee WI. Design of visible-light photocatalysts by coupling of narrow bandgap semiconductors and TiO_2: effect of their relative energy band positions on the photocatalytic efficiency. Catal Sci Technol 2013;3:1822–30.
[3] Zimmermann M, Garnweitner G. Spontaneous water release inducing nucleation during the nonaqueous synthesis of TiO_2 nanoparticles. Cryst Eng Comm 2012;14:8562–8.
[4] Liao J, He J, Xu H, Kuang D, Su C. Effect of TiO_2 morphology on photovoltaic performance of dye-sensitized solar cells:

nanoparticles, nanofibers, hierarchical spheres and ellipsoid spheres. J Mater Chem 2012;22:7910–8.
[5] Sun X, Sun Q, Li Y, Sui L, Dong L. Effects of calcination treatment on the morphology, crystallinity, and photoelectric properties of all-solid-state dye-sensitized solar cells assembled by TiO_2 nanorod arrays. Phys Chem Chem Phys 2013;15:18716–20.
[6] Cho IS, Chen Z, Forman AJ, Kim DR, Rao PM, Jaramillo TF, et al. Branched TiO_2 nanorods for photoelectrochemical hydrogen production. Nano Lett 2011;11:4978–84.
[7] Kudo A, Miseki Y. Heterogeneous photocatalyst materials for water splitting. Chem Soc Rev 2009;38:253–78.
[8] Shaislamov U, Yang BL. Single crystalline TiO_2 nanorods with enhanced visible light activity for solar hydrogen generation. Int J Hydrogen Energy 2013;38:14180–8.
[9] Sheng H, Li Q, Ma W, Ji H, Chen C, Zhao J. Photocatalytic degradation of organic pollutants on surface anionized TiO_2: common effect of anions for high hole-availability by water. Appl Catal B Environ 2013;138–139:212–8.
[10] Ochiai T, Hoshi T, Slimen H, Nakata K, Murakami T, Tatejima H, et al. Fabrication of a TiO_2 nanoparticles impregnated titanium mesh filter and its application for environmental purification. Catal Sci Technol 2011;1:1324–7.
[11] Costa RGF, Ribeiro C, Mattoso LHC. Study of the effect of Rutile/Anatase TiO_2 nanoparticles synthesized by hydrothermal route in electrospun PVA/TiO_2 nanocomposites. J Appl Poly Sci 2013;127(6):4463–9.
[12] Shibata T, Irie H, Ohmori M, Nakajima A, Watanabe T, Hashimoto K. Comparison of photochemical properties of brookite and anatase TiO_2 films. Phys Chem Chem Phys 2004;6:1359–62.
[13] Bakardjieva S, Šubrta J, Štengla V, Dianezb MJ, Sayagues MJ. Photoactivity of anatase-rutile TiO_2 nanocrystalline mixtures obtained by heat treatment of homogeneously precipitated anatase. Appl Catal B Environ 2005;58:193–202.
[14] Gao Y, Wang H, Wu J, Zhao R, Lu Y, Xin B. Controlled facile synthesis and photocatalytic activity of ultrafine high crystallinity TiO_2 nanocrystals with tunable anatase/rutile ratios. Appl Surf Sci 2014;294:36–41.
[15] Kwon SJ, Im HB, Nam JE, Kang JK, Hwang TS, Yi KB. Hydrothermal synthesis of rutile–anatase TiO_2 nano branched arrays for efficient dye-sensitized solar cells. Appl Surf Sci 2014;320:487–93.
[16] Xu F, Xiao W, Cheng B, Yu J. Direct Z-scheme anatase/rutile bi-phase nanocomposite TiO_2 nanofiber photocatalyst with enhanced photocatalytic H_2-production activity. Int J Hydrogen Energy 2014;39:15394–402.
[17] Horváth E, Kukovecz Á, Kónya Z, Kiricsi I. Hydrothermal conversion of self-assembled titanate nanotubes into nanowires in a revolving autoclave. Chem Mater 2007;19:927–31.
[18] Zhang S, Chen Q, Peng LM. Structure and formation of $H_2Ti_3O_7$ nanotubes in an alkali environment. Phys Rev B 2005;17. 014104.
[19] Palmas S, Pozzo AD, Mascia M, Vacca A, Ardu A, Matarrese R, et al. Effect of the preparation conditions on the performance of TiO_2 nanotube arrays obtained by electrochemical oxidation. Int J Hydrogen Energy 2011;36:8894–901.
[20] Zhang P, Yin S, Petrykin M, Kakihana M, Sato T. Preparation of high performance fibrous titania photocatalysts by the solvothermal reaction of protonated form of tetratitanate. J Mol Catal A 2009;309:50–6.
[21] Chen Q, Chen C, Ji H, Ma W, Zhao J. Surfactant-additive-free synthesis of 3D anatase TiO_2 hierarchical architectures with enhanced photocatalytic activity. RSC Adv 2013;3:17559–66.
[22] Ohtani B, Prieto-Mahaney OO, Li D, Abe R. What is Degussa (Evonik) P25? Crystalline composition analysis, reconstruction from isolated pure particles and photocatalytic activity test. J Photochem Photobiol A 2010;218:179–82.
[23] Lu H, Zhao B, Pan R, Yao J, Qiu J, Luo L, Liu Y, Safe and facile hydrogenation of commercial Degussa P25 at room temperature with enhanced photocatalytic activity. RSC Adv. 201; 4:1128–1132.
[24] Li G, Ciston S, Saponjic ZV, Chen L, Dimitrijevic NM, Rajh T, et al. Synthesizing mixed-phase TiO_2 nanocomposites using a hydrothermal method for photo-oxidation and photoreduction applications. J Catal 2008;253:105–10.
[25] Wang X, Pehkonen SO, Rämö J, Väänänen M, Highfield JG, Laasonen K. Experimental and computational studies of nitrogen doped Degussa P25 TiO_2: application to visible-light driven photo-oxidation of As(III). Catal Sci Technol 2012;2:784–93.
[26] Linsebigler AL, Lu G, Yates Jr JT. Photocatalysis on TiOn surfaces: principles, mechanisms, and selected results. Chem Rev 1995;95:735–58.
[27] Wu MC, Sápi A, Avila A, Szabó M, Hiltunen J, Huuhtanen M, et al. Enhanced photocatalytic activity of TiO_2 nanofibers and their flexible composite films: decomposition of organic dyes and efficient H_2 generation from ethanol–water mixtures. Nano Res 2011;4:360–9.
[28] Chen X, Mao SS. Titanium dioxide nanomaterials: synthesis, properties, modifications, and applications. Chem Rev 2007;107:2891–959.
[29] Naldoni A, D'Arienzo M, Altomare M, Marellia M, Scotti R, Morazzoni F, et al. Pt and Au/TiO_2 photocatalysts for methanol reforming: role of metal nanoparticles in tuning charge trapping properties and photoefficiency. Appl Catal B Environ 2013;130–131:239–48.
[30] Zhao D, Yang X, Chen C, Wang X. Enhanced photocatalytic degradation of methylene blue on multiwalled carbon nanotubes-TiO_2. J Colloid Interf Sci 2013;398:234–9.
[31] Dang H, Dong X, Dong Y, Huang J. Facile and green synthesis of titanate nanotube/graphene nanocomposites for photocatalytic H_2 generation from water. Int J Hydrogen Energy 2013;38:9178–85.
[32] Wu MC, Hiltunen J, Sápi A, Avila A, Larsson W, Liao HC, et al. Nitrogen-doped anatase nanofibers decorated with noble metal nanoparticles for photocatalytic production of hydrogen. ACS Nano 2011;5:5025–30.
[33] Liu Y, Zhong L, Peng Z, Cai Y, Song Y, Chen W. Self-assembly of Pt nanocrystals/one-dimensional titanate nanobelts heterojunctions and their great enhancement of photocatalytic activities. Cryst Eng Comm 2011;13:5467–73.
[34] Su R, Tiruvalam R, He Q, Dimitratos N, Kesavan L, Hammond C, et al. Promotion of phenol photodecomposition over TiO_2 using Au, Pd, and Au-Pd nanoparticles. ACS Nano 2012;6:6284–92.
[35] Ismail AA. Mesoporous PdO–TiO_2 nanocomposites with enhanced photocatalytic activity. Appl Catal B Environ 2012;117–118:67–72.
[36] Nichele V, Signoretto M, Menegazzo F, Rossetti I, Cruciani G. Hydrogen production by ethanol steam reforming: effect of the synthesis parameters on the activity of Ni/TiO_2 catalysts. Int J Hydrogen Energy 2014;39:4252–8.
[37] Chen D, Chen Q, Ge L, Yin L, Fan B, Wang H, et al. Synthesis and Ag-loading-density-dependent photocatalytic activity of Ag@TiO_2 hybrid nanocrystals. Appl Surf Sci 2013;284:921–9.
[38] Wang Y, Liu L, Xu L, Meng C, Zhu W. Ag/TiO_2 nanofiber heterostructures: highly enhanced photocatalysts under visible light. J Appl Phys 2013;113:174311–7.
[39] Roy S, Hegde MS, Ravishankar N, Madras G. Creation of redox adsorption sites by Pd^{2+} ion substitution in nanoTiO_2 for

high photocatalytic activity of CO oxidation, NO reduction, and NO decomposition. J Phys Chem C 2007;111:8153–60.
[40] Chen X, Liu L, Yu PY, Mao1 SS. Increasing solar absorption for photocatalysis with black hydrogenated titanium dioxide nanocrystals. Science 2011;331:746–9.
[41] Naldoni A, Allieta M, Santangelo S, Marelli M, Fabbri F, Cappelli S, et al. Effect of nature and location of defects on bandgap narrowing in black TiO_2 nanoparticles. J Am Chem Soc 2012;134:7600–3.
[42] Chen X, Liu L, Liu Z, Marcus MA, Wang W, Oyler NA, et al. Properties of disorder-engineered black titanium dioxide nanoparticles through hydrogenation. Sci Rep 2013;3:1510–7.
[43] Zhang J, Li M, Feng Z, Chen J, Li C. UV Raman spectroscopic study on TiO_2. I. phase transformation at the surface and in the bulk. J Phys Chem B 2006;110:927–35.
[44] Katti A, Venna SR, Carreon MA. Self-assembly hydrothermal assisted synthesis of mesoporous anatase in the presence of ethylene glycol. Catal Comm 2009;10:2036–40.
[45] Wold A. Photocatalytic properties of TiO_2. Chem Mater 1993;5:280–3.
[46] Wu MC, Chang IC, Huang WK, Tu YC, Hsu CP, Su WF. Correlation between palladium chemical state and photocatalytic performance of TiO_2-Pd based nanoparticles. Thin Solid Films 2014;570:371–5.